Journal of Solid State Electrochemistry (2021) 25:905–917
https://doi.org/10.1007/s10008-020-04858-x

ORIGINAL PAPER

Free-standing, high Li-ion conducting hybrid PAN/PVdF/$LiClO_4$/$Li_{0.5}La_{0.5}TiO_3$ nanocomposite solid polymer electrolytes for all-solid-state batteries

P. Sivaraj[1,2] · K. P. Abhilash[3] · B. Nalini[4] · P. Perumal[2] · P. Christopher Selvin[2]

Received: 12 June 2020 / Revised: 21 September 2020 / Accepted: 1 November 2020 / Published online: 16 November 2020

Abstract

The free-standing PAN/PVdF/$LiClO_4$/$Li_{0.5}La_{0.5}TiO_3$ nanocomposite solid polymer electrolytes have been prepared by solution casting technique. The thermal stability of composite solid polymer electrolytes is evaluated by TG/DSC analysis, which reveals that the filler incorporated composite samples exhibit high thermal stability up to 500 °C. The XRD analysis demonstrated that the $Li_{0.5}La_{0.5}TiO_3$ nanoparticles significantly reduced the crystallinity of the hybrid PAN/PVdF/$LiClO_4$ polymer films. The FTIR spectra of PAN/PVdF/$LiClO_4$/$Li_{0.5}La_{0.5}TiO_3$ composites show the vibrational band of –CN stretching, CF_2 asymmetric stretching, and Ti-O-La stretching which confirmed the complexation between polymer host matrices and $Li_{0.5}La_{0.5}TiO_3$ nanoparticles. The 10 wt% $Li_{0.5}La_{0.5}TiO_3$ nanoparticles embedded PAN/PVdF/$LiClO_4$ solid polymer electrolyte possessed an excellent ionic conductivity of 1.43×10^{-3} S cm^{-1} at room temperature, which is far better than the filler-free samples (~ 10^{-5} S cm^{-1}). The incorporation of $Li_{0.5}La_{0.5}TiO_3$ nanoparticles into the PAN/PVdF/$LiClO_4$ polymer electrolyte improves the concentration of free mobile lithium ions and develops Li-ion conduction channels within the crystalline framework. The PAN/PVdF/$LiClO_4$/$Li_{0.5}La_{0.5}TiO_3$ (10 wt%) composite electrolyte exhibited high thermal stability, good discharge capacities of 122, 105, 94, and 80 mAh g^{-1} at 0.1, 0.5, 1, and 2C rates, and good cycling stability.

Keywords Polymers · Nanocomposites · Electrical properties · Energy storage · All-solid-state batteries

Introduction

All-solid-state polymer batteries (ASSPBs) as an emerging battery chemistry over different energy storage devices are attractive candidate in energy storage systems and portable electronic applications due to their high flexibility, light weight, good energy/power density, and thermal stability [1, 2]. The liquid-type organic electrolytes have been used as electrolyte material in the conventional lithium-ion batteries (LIBs) [3]. The liquid electrolytes present several challenging issues, such as the formation of Li dendrite, uncontrolled side chemical reactions, and low thermal stability. It is therefore imperative to design a solid-state electrolyte to solve these problems. Substantial research efforts have been devoted to develop the solid-state electrolytes owing to their high mechanical, thermal, and dimensional stability [4, 5]. Among different solid electrolytes, the solid polymer electrolytes (SPE) possessed several advantages such as high safety due to their non-flammable character and high thermal stability. The wide electrochemical stability window of the SPE facilitates the design of high energy density ASSPBs by combining high-voltage cathode with high-capacity anode material. In addition, the SPEs that offering low manufacturing cost and high flexibility are the favourable factors for the fabrication of high performance, safe, and flexible batteries [3]. Despite numerous advantages, the solid polymer electrolytes have low ionic conductivity of 10^{-4} to 10^{-5} S cm^{-1} [4]. The ionic conductivity of SPE plays an enormous role in improving the

✉ P. Christopher Selvin
csphysics@buc.edu.in

1 Materials Research Centre, Department of Physics, N.G.M. College, Pollachi, Coimbatore, Tamil Nadu 642 001, India

2 Luminescence and Solid State Ionics Laboratory, Department of Physics, Bharathiar University, Coimbatore, Tamil Nadu 641046, India

3 Herbert Gleiter Institute of Nanoscience, Nanjing University of Science and Technology, Nanjing 210094, China

4 Department of Physics, Avinashilingam Institute for Home Science and Higher Education for Women, Coimbatore, Tamil Nadu 641 043, India

electrochemical performance of ASSPBs. It is mainly depending on the crystallinity of the solid polymer film; the high degree of polymer crystallinity mitigates the facile lithium-ion migration. To improve the electrical properties of SPE, several strategies have been explored such as incorporation of plasticizers [6], aligning polymer chains [7], cross-linking polymer with metal oxides [8], forming block copolymer [9], blending, and adding nano-inorganic ceramic fillers into a polymer matrix [10]. Among these techniques, the blending of two different polymer hosts and the incorporation of ceramic fillers are effective strategies to improve the ionic conductivity and mechanical and thermal stability of the SPE.

Several polymers such as polyethylene oxide (PEO) [11], polyimide (PI) [12], polymethyl methacrylate (PMMA) [13], poly(vinyl chloride) (PVC) [12], poly(urethane) (PU) [14], polyacrylonitrile (PAN) [15], and polyvinylidene fluoride (PVdF) [16] have been widely studied as polymer electrolytes for lithium polymer batteries. Among those polymers, the PAN and PVdF are the promising host polymer matrices. The PAN possessed high ionic conductivity and stable electrochemical performance due to its strong molecular interaction between lithium-based salt and nitrile C≡N functional groups present in PAN polymer matrix [17]. Nonetheless, a major drawback of the PAN-based polymer electrolyte is poor mechanical and thermal stability and low film-forming capability, which limits the widespread use of practical lithium-ion batteries. The PVdF presents numerous features such as good electrochemical stability, good dielectric constant ($\varepsilon = 8.4$), affinity to the electrolyte solution, and strong electron-withdrawing molecular group (-C-F-) [18]. In spite of its features, the addition of PVdF decreases the ionic conductivity due to the crystalline nature of PVdF. As a result, a variety of methods have been attempted to solve these problems by incorporating inorganic nanofillers such as TiO_2, SiO_2, Al_2O_3, and Sm_2O_3 $Li_{1.3}Al_{0.3}Ti_{1.7}(PO_4)_3$ to the polymer matrix [19]. The incorporation of nanofiller in the polymer electrolytes significantly enhanced ionic conductivity, mechanical strength, thermal stability, and compatibility with electrode-electrolytes [20]. Additionally, the introduction of nanoparticles distorts the arrangement of the polymer chain, which leads to the improvement of more free volume or amorphous region for ionic transport.

So far, the nanocomposite solid polymer electrolytes have been prepared by incorporating nanofillers into a single polymer host matrix. There are no studies on nanocomposite polymer electrolyte preparation by mixing two promising polymer host matrices with ceramic nanofillers to produce solid polymer electrolyte for ASSPBs. In this work, an effort has been made to blend two promising polymers (PAN and PVdF) with highly Li-ion conducting (10^{-3} S cm^{-1}) [21] $Li_{0.5}La_{0.5}TiO_3$ (LLTO) perovskite nanoparticles as active filler in the hybrid polymer host matrices. The blending of PAN with PVdF matrix and LLTO nanoparticles greatly enhances the thermal stability and ionic conductivity of the composite samples. A Swagelok-type ASSPBs have been assembled by combining the high-capacity cathode (Li_2FeSiO_4/C), the PAN/PVdF/$LiClO_4$/LLTO nanocomposite as solid electrolyte cum separator, and Li-metal as anode. The ASSPBs exhibit good electrochemical stability window and cycling performance.

Experimental details

Preparation of $Li_{0.5}La_{0.5}TiO_3$ nanoparticles

The LLTO nanoparticles were prepared by sol-gel method as reported in a previous work [22]. Lithium nitrate (AR-99.5%, Aldrich), lanthanum nitrate hexahydrate (AE-99%, Himedia), tetrabutyl titanate (AR-99%, Aldrich), and acetylacetone (acac) (AR-99%, Himedia) were used as the raw materials. The $LiNO_3$ and $La(NO_3)_3.6H_2O$ were weighed in terms of the stoichiometric composition, $Li_{0.5}La_{0.5}TiO_3$, and dissolved in ethylene glycol monomethyl ether and afterwards they were mixed with the mixture solution of tetra butyl titanate and acetylacetone. The precursor sol-gel was calcined at 900 °C for 6 h to yield pure $Li_{0.5}La_{0.5}TiO_3$ (LLTO) white powder.

Preparation of PAN/PVdF/$LiClO_4$/LLTO nanocomposite solid polymer electrolytes

The PAN/PVdF/$LiClO_4$ hybrid polymer films were prepared by solution casting method [23, 24]. The PVdF (SR, 95), PAN (Sigma-Aldrich, 99%), and $LiClO_4$ (Sigma-Aldrich, 99.8%) were used as raw materials for the preparation. The DMF was used as the solvent for the sample preparation. After various trial and errors, the optimum composition of $LiClO_4$ and PVdF was fixed as 15 wt% and 10 wt% for all the samples. The 10 wt% of PVdF, 15 wt% of $LiClO_4$, and 75 wt% of PAN were dissolved in 20-ml DMF solvent and stirred for 6 h on a magnetic stirrer. Then, the solution was poured into a glass Petri dish and kept in an incubator oven at 80 °C over 12 h for solvent evaporation to obtain a free-standing polymer film as depicted in the schematic diagram shown in Fig. 1a. The similar procedure was followed for the preparation of the PAN/PVdF/$LiClO_4$/LLTO nanocomposite solid polymer films with different composition of LLTO nanoparticles. The composition and designation of the samples are presented in Table 1.

Characterization of the polymer electrolytes

The thermal stability of the PAN/PVdF/$LiClO_4$/LLTO composite solid polymer electrolytes was carried out using thermogravimetric (TG) analyser (DTA-60AH) and differential scanning calorimetric analyser (DSC7, Perkin-Elmer instrument). It was performed from room temperature to 700 °C at a heating rate of 10 °C/min. Structural characterization of the

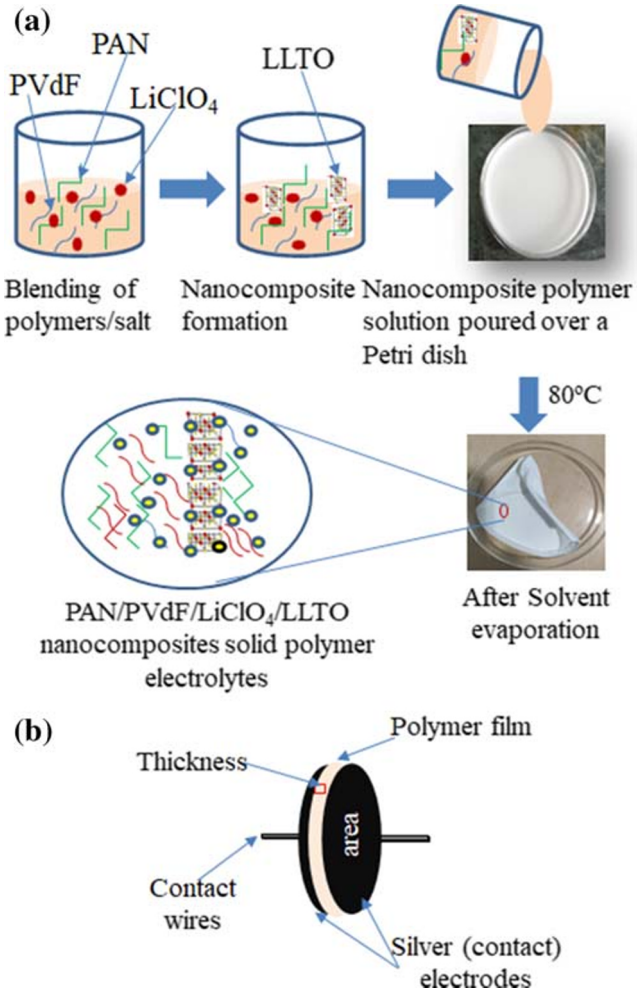

Fig. 1 (**a**) The schematic representation of the preparation of nanocomposite solid polymer electrolytes via solution casting method and (**b**) the experimental setup for the impedance measurement

composite solid polymer electrolyte was carried out by powder XRD (XRD-Shimazdu-6000) analysis. The vibration spectrum of the sample was analysed by the FTIR (SHIMAZDU 220-93270-55 IRTracer-100) analysis. Morphology of the polymer film was analysed by scanning electron microscopy (SEM) (JEOL-JSM 6390) analysis. The ionic conductivity of the sample was measured by complex impedance spectrometer (HIOKI LCR 3532-50; frequency range: 42 Hz to 5 MHz with fixed voltage of 0.5 V). The solid polymer films were sandwiched between two silver blocking electrodes as depicted in Fig. 1b. A symmetric cell (ss|polymer electrolyte|ss) has been fabricated using solid polymer electrolyte and stainless-steel blocking electrodes. The cell ss|polymer electrolyte|ss was used to test the electrochemical stability window of the polymer electrolyte. The linear sweep voltammetry (LSV) was performed within a potential range of 1 to 5 V (Biologic, SP 150).

Electrochemical characterization

In this work, Li_2FeSiO_4/C [25] was used as cathode material, and the filler-free, best-performing PAN/PVdF/$LiClO_4$/LLTO was employed as solid polymer electrolyte cum separator and graphite/Li-metal foil as anode.

Electrode fabrication

The 80 wt% of Li_2FeSiO_4/C, 10 wt% of PVdF binder, and 10 wt% of carbon additives were dissolved in the N-methyl-2-pyrrolidone (NMP) solvent and stirred for 6 h. The resultant solution was coated uniformly on a clean aluminium foil by doctor blade method and kept in a hot air oven at 120 °C overnight. To investigate the redox property of the all-solid-state battery, the electrochemical cell was fabricated by sandwiching composite solid polymer electrolyte between the Li_2FeSiO_4/C and graphite as cathode and anode materials. The cyclic voltammetry (CV) was performed for 50 cycles within the potential range of 1.55 V at a sweeping rate of 10 mV s^{-1} using an electrochemical workstation (Biologic, SP 150). To carry out the galvanostatic charge and discharge test, a Swagelok cell type all-solid-state electrochemical cell was fabricated by sandwiching PAN/PVdF/$LiClO_4$/LLTO between lithium foil anode (reference electrode) and Li_2FeSiO_4/C cathode (working electrode) in an argon filled glovebox. Galvanostatic charge-discharge tests were carried out using a battery tester (LAND (CT2001A)) at various C rates (0.1, 0.5, 1, and 2C) within the voltage range of 1.5 to 4.8 V versus Li^+/Li.

Table 1 Compositions and designation of the PAN/PVdF/$LiClO_4$/LLTO nanocomposites

Sample designation	PAN (g/wt%)	PVdF (g/wt%)	$LiClO_4$ (g/wt%)	LLTO (g/wt%)
PAN/$LiClO_4$	0.85/85	0.0	0.15/15	0.0
PAN/PVdF/$LiClO_4$	0.75/75	0.1/10	0.15/15	0.0
PAN/PVdF/$LiClO_4$/LLTO: 5 wt%	0.70/70	0.1/10	0.15/15	0.05/5
PAN/PVdF/$LiClO_4$/LLTO: 10 wt%	0.65/65	0.1/10	0.15/15	0.10/10
PAN/PVdF/$LiClO_4$/LLTO: 15 wt%	0.60/60	0.1/10	0.15/15	0.15/15
PAN/PVdF/$LiClO_4$/LLTO: 20 wt%	0.55/55	0.1/10	0.15/15	0.20/20

Results and discussion

Thermal, structural, and morphological characterizations

Thermal analysis of the PAN/PVdF/$LiClO_4$/LLTO blend composite solid polymer electrolytes has been performed by thermogravimetric (TG) and differential scanning calorimetry (DSC) techniques [26] from room temperature to 700 °C. Figure 2i (a) shows the DSC curve of PAN/$LiClO_4$, in which exothermic and endothermic peaks were observed at 171 and 275 °C. The peak at 171 °C is due to the crystallization of the PAN host matrix, and peak at 275 °C is ascribed to the decomposition of the PAN/$LiClO_4$ complex [15]. The PVdF blended PAN/$LiClO_4$ sample exhibits a sharp exothermic peak at 173 °C, which is due to the crystallization of PVdF matrix (Fig. 2i (b)). The PAN/PVdF/$LiClO_4$ complex shows an endothermic peak at 330 °C due to the decomposition of the blended complex polymer film. It reveals that the PVdF-embedded sample shows better thermal stability when compared with the PAN/$LiClO_4$ polymer electrolytes. The DSC curve of 5 wt% LLTO-incorporated solid polymer electrolyte is shown in Fig. 2ii (c). The two endothermic peaks observed at 335 °C and 477 °C correspond to the melting of polymer hosts and filler complex. These peaks are more prominent in the 10 wt% LLTO filler added sample which is due to the strong interaction between nanofiller and the PAN/PVdF/$LiClO_4$ complex system. Moreover, the melting temperature of composite polymer films increases with increase in the composition of LLTO nanoparticles (Fig. 2ii (d–f), which indicates that the polymer films are thermally stable up to 500 °C.

The TG curve of PAN/$LiClO_4$ polymer film exhibits significant weight decay in the tested temperature range which involves two thermal events (Fig. 2iii (a)). The first weight loss around 16.43% from room temperature (RT) to 130 °C is assigned to the evaporation of low molecular weight components and the solvent (DMF) groups. The second weight loss of about 71.19% in steep slope for PAN host matrix, observed from 310 to 540 °C, is attributed to the decomposition of the main polymer chain and cross-linking bridge. The weight decay of PVdF-embedded PAN/$LiClO_4$ polymer film exhibits three thermal events, first weight loss of 10.25% due to evaporation of residual solvents and second decay of 10.77% from 310 to 400 °C (approximately) due to the decomposition of PAN/$LiClO_4$ system. In the temperature between 310 and 540 °C, PAN/PVdF/$LiClO_4$ shows a sharp weight loss about 47.97% which can be ascribed to the melting of the complex system (Fig. 2iii (b)). Compared with PAN/$LiClO_4$, the PVdF-incorporated PAN/$LiClO_4$ complex system exhibited better thermal stability. Figure 2 iv shows the TG curve of PAN/PVdF/$LiClO_4$/LLTO nanocomposite solid polymer electrolytes. All the composite samples possessed three stage of weight loss from room temperature to 700 °C. It should be noted that all samples experience a gradual weight loss between 4.39 and 7.09% in the temperature range of 30–130 °C

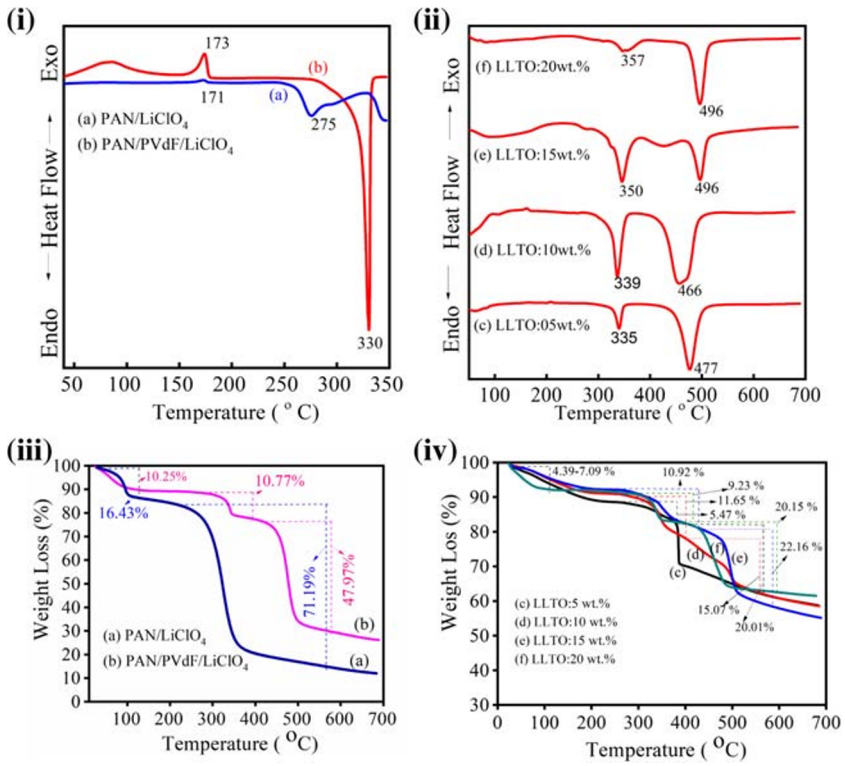

Fig. 2 The DSC curves of PAN/$LiClO_4$ and PAN/PVdF/$LiClO_4$ complex (**i**) and PAN/PVdF/$LiClO_4$ with the addition of different composition of LLTO nanoparticles (**ii**). The TGA curves of PAN/$LiClO_4$ and PAN/PVdF/$LiClO_4$ complex (**iii**) and PAN/PVdF/$LiClO_4$ with the addition of different quantity of LLTO nanoparticles (**iv**)

corresponding to the evaporation of water molecules and solvents, and second step between 300 and 400 °C is attributed to the degradation of lithium salt ($LiClO_4$) [27]. The final step weight decay (between 15.07 and 22.16%) for all the composite films is observed between 400 and 540 °C, which corresponds to the degradation of polymer host matrices [27]. It resembles that the weight loss of PAN/PVdF/$LiClO_4$/LLTO is comparatively lower than filler-free samples, which is a clear indication of excellent thermal stability of the LLTO-incorporated composites. The obtained thermal stability of the PAN/PVdF/$LiClO_4$/LLTO is far better than the previous report [28].

The XRD pattern of the PAN/PVdF/$LiClO_4$/LLTO nanocomposite solid polymer electrolyte is shown in Fig. 3. The PAN/$LiClO_4$ sample shows a sharp diffraction peak at 2θ = 17° and a broad hike at 2θ around 20 to 30° (Fig. 3a). The crystalline peak at $2\theta = 17°$ is indexed to (010) crystallographic plane of PAN host matrix [29]. The PVdF-incorporated PAN/$LiClO_4$ exhibits a crystalline peak at $2\theta = 20.5°$ ascribed to the 110/200 reflection of the orthorhombic β-phase PVdF and a smaller broad peak observed at 38.9° corresponding to (002) reflection of the monoclinic α-phase [30, 31]. The blending of PVdF with PAN/$LiClO_4$ system exhibited the semicrystalline phase of both PVdF and PAN polymers with a slightly widened peak at $2\theta = 17°$, indicating the mixing of the polymer host matrices as shown in Fig. 3b. The diffraction peaks of polymer hosts are broader and less prominent after the addition of 5 wt% of LLTO nanoparticles (Fig. 3c) when compared with the PAN/PVdF/$LiClO_4$ complex. The crystalline peak of the PAN and PVdF polymer is suppressed with the addition of 10 wt% LLTO nanoparticles. Further increasing the concentration of LLTO filler (20 wt%), the XRD pattern exhibits the emergence of

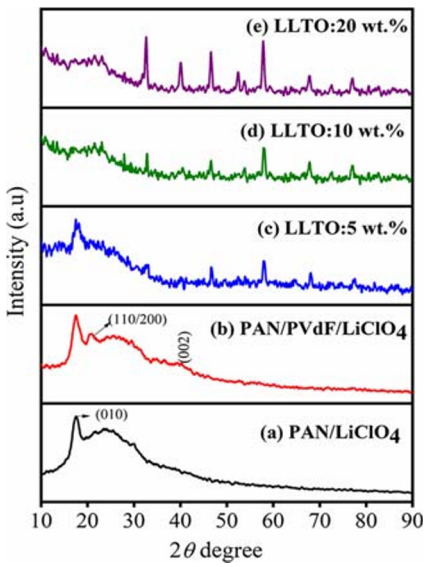

Fig. 3 The XRD pattern of PAN/PVdF/$LiClO_4$/LLTO composite solid polymer electrolytes

several crystalline peaks at $2\theta = 32.86$, 40.01, 46.51, 52, 58, 67, and 77°, which are assigned to (110), (111), (200), (211), (220), and 310 crystallographic planes of the cubic perovskite structure of LLTO [22]. All the diffraction peaks of LLTO are well matched with the PCPDF data (PCPDF Card No: 053-0109). The characteristic peaks of PAN/PVdF/$LiClO_4$ complex completely suppressed due to the predominant composition of LLTO, as evidenced from the XRD pattern. The degree of crystallinity has been calculated from the XRD pattern using Eq. (1) [10]:

$$\text{Degree of crystallinity} = \frac{A_c}{A_c + A_a} \quad (1)$$

where A_c is the integrated area of crystalline phase and A_a is the area of amorphous region. The degree of crystallinity is calculated as 42.29, 46.14, 10.58, 9.75, and 16.27% for PAN/$LiClO_4$, PAN/PVdF/$LiClO_4$, 5, 10, and 20 wt% LLTO embedded PAN/PVdF/$LiClO_4$ composite polymer electrolytes. It implies that the degree of crystallinity of the polymers decreases with increase in the concentration of the LLTO nanoparticles. However, high quantity of filler addition exhibits its own crystalline phase, which is not favourable for ionic migration in the composite polymer electrolytes [10].

The FTIR characterization was conducted to explore the nature of bonding and different functional groups present in polymer electrolytes by measuring the molecule's vibrational bands. The characteristic vibrational band of the PAN is observed at 2246, due to stretching vibration of −CN bond [29] (Fig. 4i (a)). The bands at 2934 cm^{-1} and 1634 cm^{-1} are attributed to the symmetrical $-CH_2$ and asymmetrical −CH stretching vibrations of PAN [32]. The PAN/$LiClO_4$ also consists of $-CH/CH_2$ deformation vibrations in the frequency range of 1240–1460 cm^{-1} [33]. The band located at 622 cm^{-1} is attributed to the stretching vibration of ClO_4^- group [34]. The PVdF-incorporated PAN/$LiClO_4$ polymer film exhibits a characteristic band at 545 cm^{-1}, due to the CH_2 rocking vibrations of PVdF (Fig. 4i (b)). The rocking modes of CF_2 vibration of β-phase are obtained at 836 and 873 cm^{-1} [35]. The vibration mode noticed at 1090 cm^{-1} is assigned to asymmetric stretching vibration of C–C backbone. The frequency bands at 1164 cm^{-1} and 1238 cm^{-1} are due to asymmetric stretching of CF_2 and symmetric stretching mode of C–C [35, 36]. A peak originated at 1402 cm^{-1} is attributed to the CF_2 bending mode [32]. The stretching vibration of free ClO_4^- is shifted to 652 cm^{-1} when blending the PVdF with PAN/$LiClO_4$ system. The vibrational band located at 3567 cm^{-1} is the result of the O–H stretching vibration that originates from the adsorbed water molecule observed in the air [37–39].

The incorporation of LLTO nanoparticles significantly amend the molecular interaction between the PVdF, PAN, and $LiClO_4$, shown in Fig. 4i (c). The strong characteristic

vibrational band observed at 1040 cm^{-1} is due to the bending vibration of Ti–O–La functional group in the LLTO nanofiller [40, 41]. The IR bands of CH_2 and CF_2 vibrations are almost similar to the filler-free polymers after the addition of 5 wt% LLTO nanoparticles. As a result, the disappearance of 836, 873, and 1090 cm^{-1} bands and the emergence of a band at 1040 cm^{-1} revealed the rupture of CF_2 and C–C bonds and the generation of Ti–O–La molecular bonds. The incorporation of nanofiller into the polymer/salt system slightly decreased the intensity of CH_2 stretching vibration but does not change the characteristic stretching vibration (−C≡N) of PAN. Figure 4 ii shows enlarged FTIR spectra for the composite samples which is a clear indication of emergence of the peak at 1040 cm^{-1} with the addition of LLTO nanoparticles. It reveals that the nanofiller is perfectly embedded into the blended solid polymer electrolytes. The dissolution of the $LiClO_4$ salt in the polymer host plays crucial role in determining the ionic conductivity of the electrolytes. The vibrational mode of free

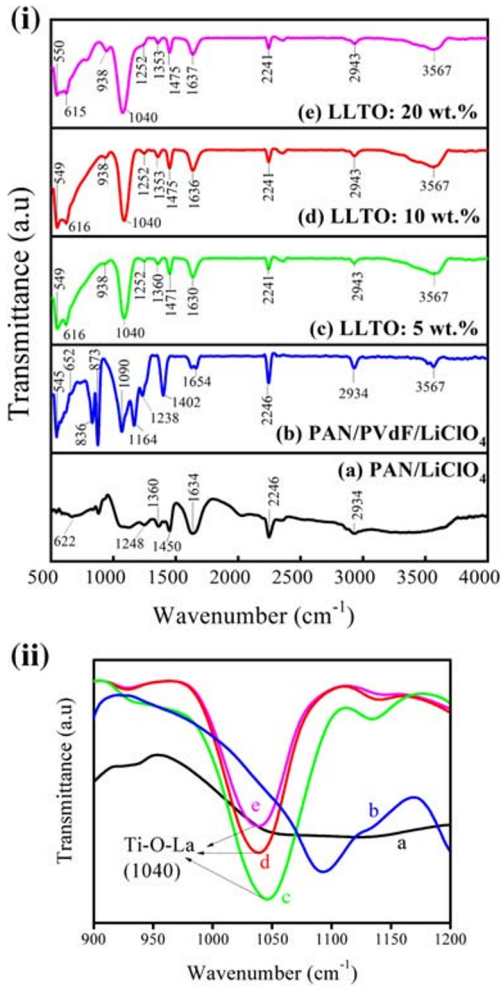

Fig. 4 (**i**) The FTIR spectra of PAN/PVdF/$LiClO_4$/LLTO composite solid polymer electrolytes and (**ii**) enlarged FTIR spectra (900–1200 cm^{-1}) which is the clear indication of the emergence of characteristic vibrational peak (1040 cm^{-1} ~Ti-O-La) of LLTO after incorporation of LLTO nanoparticles

ClO_4^- and ion-pair formation are observed in the frequency range of 615–633 cm^{-1} [34]. Theses peaks are more prominent with the addition of LLTO, which represents that the dissolution of $LiClO_4$ increases with increasing the concentration of LLTO nanofiller. The FTIR result implies that LLTO nanoparticles are strongly interlinked with polymer matrices, which establish the perfect mixing of PVdF, PAN, and LLTO nanoparticles.

Figure 5 a and b show the SEM micrograph of the PAN/$LiClO_4$ and PAN/PVdF/$LiClO_4$ solid polymer films. The particles are not uniformly distributed over the surface of the sample, and the individual particles are not visible in the micrographs. The incorporation of LLTO nanoparticles into the PAN/PVdF/$LiClO_4$ composites has changed the morphology of the solid polymer electrolyte. The particles are more or less uniformly spread over PAN/PVdF/$LiClO_4$ complex, with the addition of 10 wt% of the LLTO filler as shown in Fig. 5c. The LLTO nanoparticles incorporated into the hybrid polymer salt complex does not display any pores, cavities, or pinholes over the surface. Figure 5 d shows the SEM micrograph of 20 wt% LLTO added PAN/PVdF/$LiClO_4$, which exhibits the highly aggregated nanoparticles with micropores. The predominant composition of LLTO results in non-uniform morphology with the aggregation of nanoparticles. The SEM result has shown that the morphology of polymer film is tailored to the combination of PVdF and PAN/$LiClO_4$ with the optimum composition of LLTO nanoparticles that influence the electrochemical properties of composite solid polymer electrolytes.

Conductivity study

The complex impedance spectroscopy was used to assess the ionic conductivity of solid polymer electrolytes. The Nyquist plot of PAN/PVdF/$LiClO_4$/LLTO composite solid polymer electrolytes is depicted in Fig. 6i (a–f). It was fitted by Z-View software with most suited equivalent circuit display best-fit results, and the fitted parameters are listed in Table 2. The equivalent circuit model in Fig. 6i (inset picture) consists of a parallel combination of R_b and CPE-1 elements with one CPE-2 element in series, which are attributed to the bulk and electrolyte/contact electrodes contributions. Here R denotes a resistance and CPE is the constant phase element. The Rs indicates the shunt resistance or contact resistance, and Rb is the bulk resistance, which can be used to obtain the ionic conductivity. The constant phase elements were used as an alternative to pure capacitors due to the presence of depressed semicircles. In this scenario, the CPE-2 is used to boost the fit of the low-frequency electrode, and spike refers to the blocking effect of contact electrodes and polymer films. The ionic conductivity of the solid polymer electrolytes is obtained using the following equation:

$$\sigma = d/(A \times R_b) \tag{2}$$

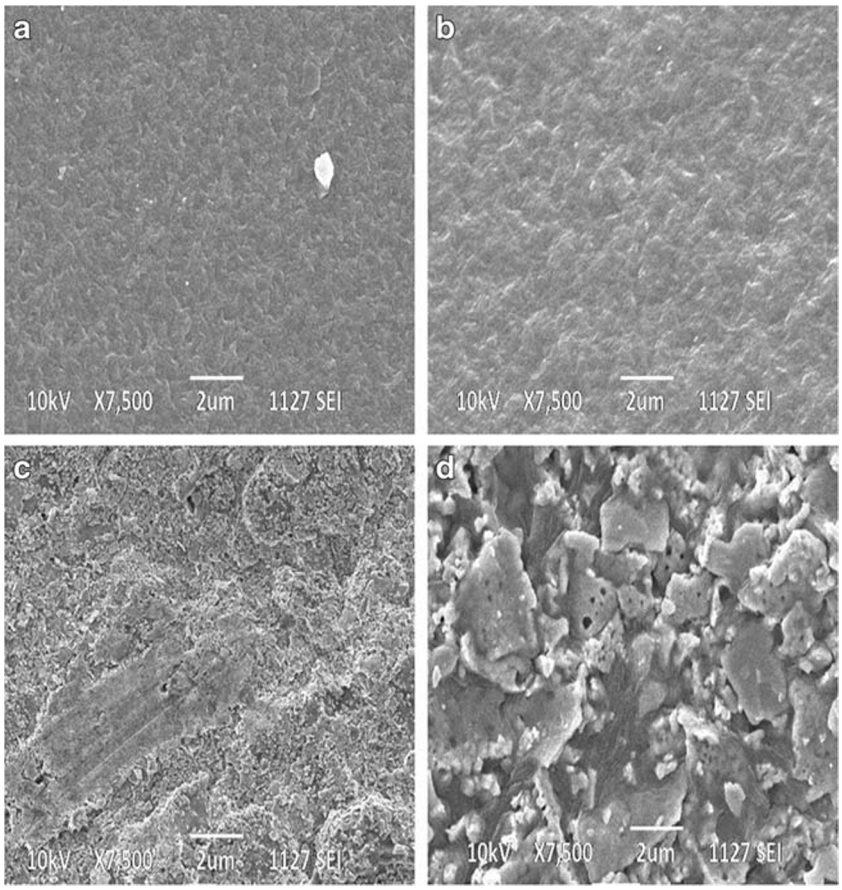

Fig. 5 The SEM micrographs of the composite polymer electrolytes: (**a**) PAN/$LiClO_4$, (**b**) PAN/PVdF/$LiClO_4$, (**c**) PAN/PVdF/$LiClO_4$/LLTO (10 wt%), and (**d**) PAN/PVdF/$LiClO_4$/LLTO (20 wt%)

where σ is ionic conductivity (S cm^{-1}), d is the thickness of the sample, A is area of the polymer electrolyte, and R_b is the bulk resistance. The PAN/$LiClO_4$ polymer film shows a depressed semicircle at high-frequency and a spike at low-frequency region (Fig. 6i (a)). The high-frequency semicircle indicates the bulk resistance of polymer films, and the straight line at low frequency is attributed to the ion blocking at contact electrodes [42, 43]. The total conductivity of PAN/$LiClO_4$ is found to be 4.17×10^{-5} S cm^{-1}. The incorporation of PVdF into PAN/$LiClO_4$ complex increased the diameter of the semicircle due to the high bulk resistance of the sample, shown in Fig. 6i (b). The ionic conductivity of PAN/PVdF/$LiClO_4$ sample is 2.23×10^{-5} S cm^{-1} which is comparatively lower than PAN/$LiClO_4$ salt complex. Hence, the low ionic conductivity of PAN/PVdF/$LiClO_4$ hybrid polymer film has been improved by incorporating different wt% of LLTO nanoparticles. The bulk conductivity of 5 wt% LLTO nanoparticles embedded PAN/PVdF/$LiClO_4$ is 1.08×10^{-4} S cm^{-1} which is one order of magnitude higher than that of the filler-free samples.

It is interesting to note that the 10 wt% LLTO nanoparticles incorporated PAN/PVdF/$LiClO_4$ composite exhibits a small depressed semicircle at high-frequency region with a low-frequency spike (Fig. 6i (d)). It delivers an excellent ionic conductivity of 1.43×10^{-3} S cm^{-1}, which is far better than the PAN/PVdF/$LiClO_4$ polymer electrolyte ($\sim 10^{-5}$ S cm^{-1}). This is due to the rapid Li-ion migration through the smooth surfaces of polymer/LLTO nanoparticles that serve as a conductive network within the complex polymer matrices. It shows that the nanofiller plays a crucial role for separating Li^+ and ClO^-_4 in composite solid polymer electrolytes. In addition, the Lewis acid-base theory [44] describes the improvement of the ionic conductivity with the incorporation of LLTO nanoparticles. The heavy molecular interaction in the metal oxide nanoparticles between the ClO^-_4 and acid groups separate Li^+ and ClO^-_4 from the $LiClO_4$ salt of the polymer electrolytes producing large number of free Li-ions [45]. The Li-ions migrate easily through the increased free volume or flexible-amorphous backbone of PAN/PVdF hybrid polymer electrolyte and through the crystalline LLTO perovskite structure [46, 47], which is schematically represented in Fig. 6ii. The incorporation of filler with optimum composition significantly reduce the crystallinity of the polymers and enrich the amorphous nature of polymer host matrices, which reflects in the enhancement of ionic conductivity. Mariano Romero et al. [48] reported that the composite LLTO-PMMA provides an ionic conductivity of 1.13×10^{-4} S cm^{-1}. Chunsheng et al. [49] demonstrated that the 20 wt% $Li_{0.55}La_{0.35}TiO_3$ fibre embedded in PEO-

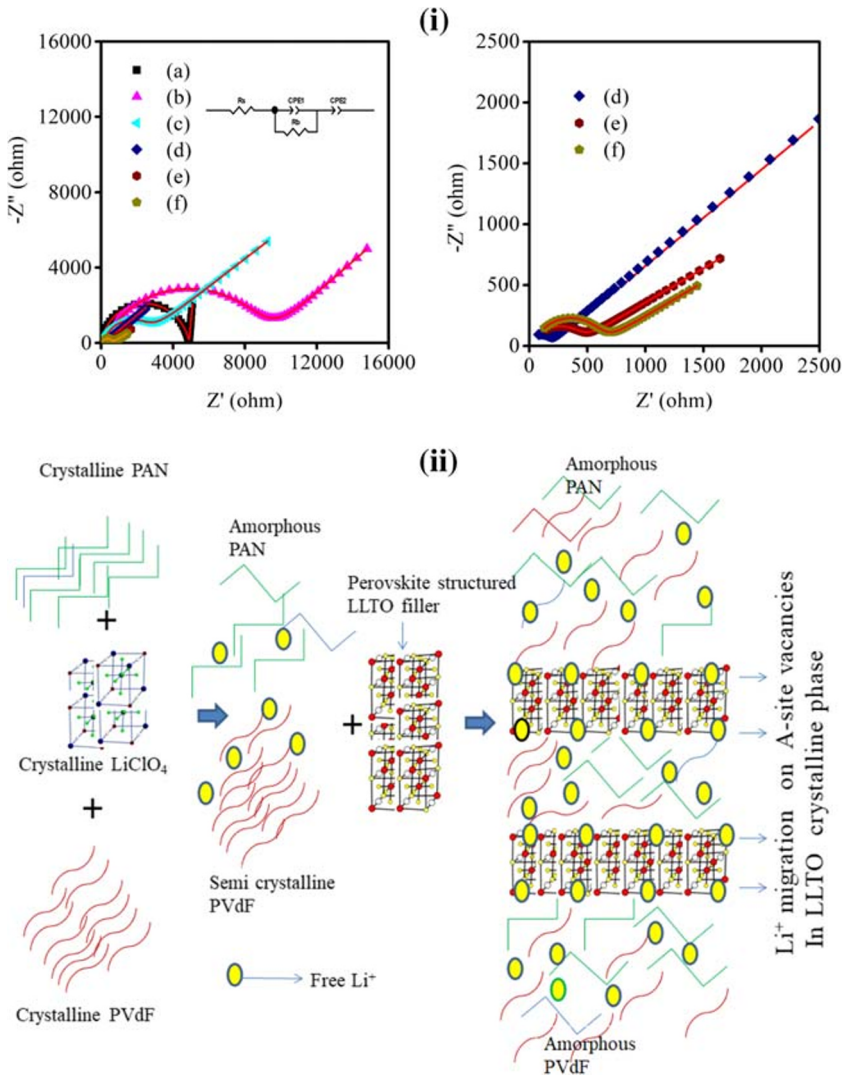

Fig. 6 (**i**) The Nyquist plots of the solid polymer electrolytes: (a) PAN/$LiClO_4$, (b) PAN/PVdF/$LiClO_4$, and PAN/PVdF/$LiClO_4$/LLTO composite polymer electrolytes with different concentration of LLTO nanoparticles. (c) LLTO, 5 wt%; (d) LLTO, 10 wt%; (e) LLTO, 15 wt%; and (f) LLTO, 20 wt%. (ii) The schematic representation of Li-ion migration in the PAN/PVdF/$LiClO_4$/LLTO composite polymer electrolytes, in which the Li-ions migrate through A-site vacancies in the perovskite structure of LLTO nanofiller and enriched amorphous region of PAN and PVdF host matrices

$LiN(SO_2CF_2CF_3)_2$ composite system exhibited a highest ionic conductivity of 5.0×10^{-4} S cm^{-1} at room temperature. Wei Liu et al. [50] prepared 15 wt% $Li_{0.33}La_{0.557}TiO_3$ nanowire incorporated in PAN/$LiClO_4$ and reported the ionic conductivity of 2.4×10^{-4} S cm^{-1}. In the present work, the obtained ionic conductivity is far better than the previous reports

Table 2 The complex impedance fitted parameters, calculated ionic conductivity, and activation energy of the PAN/PVdF/$LiClO_4$/LLTO composite polymer electrolytes

Sample	PAN/$LiClO_4$	PAN/PVdF/$LiClO_4$	PAN/PVdF/$LiClO_4$/LLTO			
			5 wt%	10 wt%	15 wt%	20 wt%
CPE-1 (F)	1.61×10^{-9}	3.08×10^{-9}	11.25×10^{-9}	26.5×10^{-9}	20.86×10^{-9}	19.5×10^{-9}
n	0.90	0.7	0.90	0.98	0.8	0.83
Bulk resistance R_b (Ω)	4890	8956	1956	145	356	557
CPE-1 (F)	3.345×10^{-6}	4.13×10^{-6}	12.93×10^{-6}	34.87×10^{-6}	0.13×10^{-6}	0.176×10^{-6}
n	0.94	0.45	405	0.42	0.32	0.334
Thickness (mm)	0.51	0.50	0.53	0.52	0.49	0.52
Ionic conductivity (S/cm)	4.17×10^{-5}	2.23×10^{-5}	1.08×10^{-4}	1.43×10^{-3}	5.50×10^{-4}	3.73×10^{-4}
Activation energy (eV)	0.48	0.50	0.34	0.29	0.30	0.33

[48–50]. Figure 6 i (e and f) displays the 15 and 20 wt% LLTO nanoparticles embedded PAN/PVdF/$LiClO_4$ composite polymer films. When dispersing high quantity of LLTO nanoparticles, the diameter of the depressed semicircle increased, which significantly reduced the ionic conductivity of composite samples. The low ionic conductivity can be attributed to the highly agglomerated morphology, aggregation of ions, and high crystallinity of the LLTO nanoparticles. The calculated ionic conductivity of the samples is listed in Table 2. It reveals that the high content of filler addition exhibits its own crystalline phase, which is not in favour of ionic migration within the composite polymer electrolytes.

The temperature-dependent conductivity analysis of the PAN/PVdF/$LiClO_4$/LLTO samples has been carried out between 30 and 200 °C and depicted in Fig. 7. This shows two linear regions between 30–125 °C and 125–200 °C that are involved in ion migration due to specific activation energy. Across all samples, the conductivity plots show a linear behaviour within the temperature range of 25 to 125 °C. The linear behaviour (25 to 125 °C) is ascribed to the freezing point of carbonate solvent in the electrolyte and melting of the crystalline phase of PAN host matrix. It indicates that the amorphous phase provides fast lithium-ion transport in the polymer host network, and it further establishes facile conduction pathway in the polymer electrolyte which increases the hopping conduction activity [51]. As seen from Fig. 7, the linear region in the log(σ) vs 1/T plots is slightly bent above the temperature 125 °C. This non-linear behaviour follows the Vogel-Tamman-Fulcher (VTF) relation [10, 52] which can be used to obtain the activation energy (E_a) of ionic conduction instead of Arrhenius model at high temperatures. The non-linear temperature-dependent conductivity can be expressed as per the VTF model as given below [52]:

$$\sigma = AT^{-1/2}\exp\left(\frac{-E_a}{T-T_o}\right) \tag{3}$$

where A is a pre-exponential factor, E_a is the activation energy, T is temperature in kelvin (K), and T_o is equilibrium glass transition temperature close to T_g. The warped linear behaviour at high temperatures promotes the segmental movement of polymer chains, which enhances the conductivity of Li-ion in the polymer composite electrolytes. The thermal activation favours the movement of ions at the higher temperatures in combination with the segmental motion of the polymer chain. The high ionic conductivity of the sample at high temperature can be attributed to the large bond rotation with increase in the temperatures [53]. In the present study, the obtained highest ionic conductivity can be attributed to the blending of thermally stable PVdF with high Li-ion conducting PAN/$LiClO_4$ and LLTO nanoparticles.

The PAN delivers large-scale segmental motion of the polymer chain [50]. The PVdF, as an inert host, provides high thermal and mechanical power to PAN/$LiClO_4$ polymer films. Therefore, the promising properties of both PAN and PVdF host polymers are used to design a hybrid polymer matrix. Further, its electrical and thermal stability has been systematically enhanced through the incorporation of LLTO nanofiller. The calculated activation energy for all the samples is listed in Table 2. Compared with other samples, the optimum composition of 10 wt% LLTO nanoparticles embedded PAN/PVdF/$LiClO_4$ exhibited lower activation energy of 0.29 eV. The low activation energy and high ionic conductivity are due to the high surface area of nanofillers and enhanced amorphous region of the polymer host matrices [46, 47, 54].

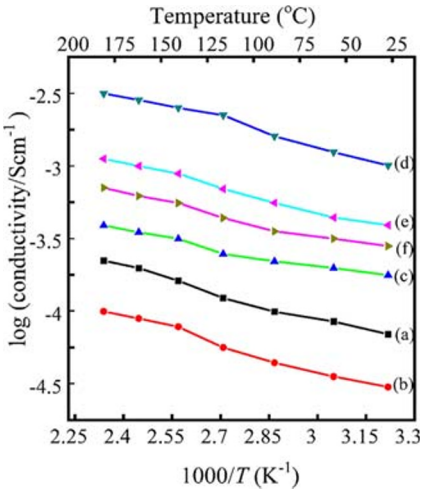

Fig. 7 The ionic conductivity vs 1000/T plot of the PAN/PVdF/$LiClO_4$/LLTO composite solid polymer electrolytes: (a) PAN/$LiClO_4$, (b) PAN/PVdF/$LiClO_4$, and PAN/PVdF/$LiClO_4$/LLTO composite polymer electrolytes with different concentration of LLTO nanoparticles. (c) LLTO, 5 wt%; (d) LLTO, 10 wt%; (e) LLTO, 15 wt%; and (f) LLTO, 20 wt%

Electrochemical characterizations

The electrochemical stability of solid polymer electrolytes plays a major role in enhancing the operating voltage and energy density of all-solid-state batteries. The electrochemical stability window of the filler-free PAN/PVdF/$LiClO_4$ and the best-performing PAN/PVdF/$LiClO_4$/LLTO (10 wt%) composite polymer electrolytes has been determined using the linear sweep voltammetry (LSV) technique (Fig. 8a) in the potential range of 1–5 V at a sweep rate of 10 mV s^{-1}. The electrochemical stability window voltage of the solid polymer electrolyte is obtained as 3.97 and 4.89 V for the PAN/PVdF/$LiClO_4$ and PAN/PVdF/$LiClO_4$/LLTO (10 wt%) composites, respectively. The result shows that the electrochemical stability of the PAN/PVdF/$LiClO_4$ electrolyte is greatly enhanced by incorporating an appropriate amount of (10 wt%) LLTO nanoparticles, which is far better than the previous work [55]. The operating potential of practical lithium-ion batteries ranges from 1.8 to 3.5 V [56]. In this work, the PAN/PVdF/

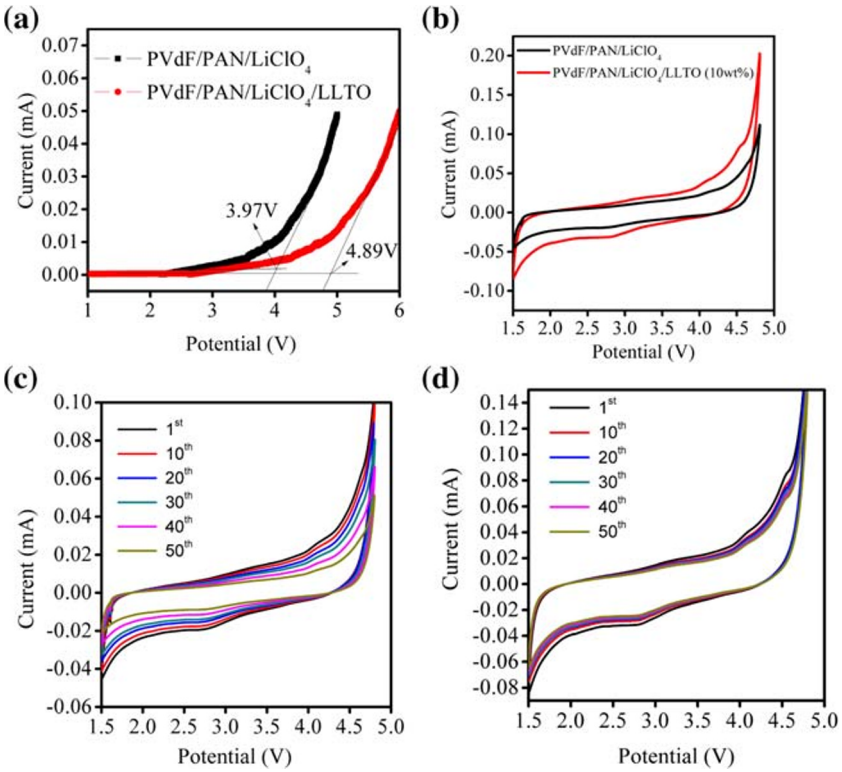

Fig. 8 **a** The linear sweep voltammetry profile of PAN/PVdF/$LiClO_4$ and best-performing PAN/PVdF/$LiClO_4$/LLTO (10 wt%) composite polymer electrolytes, (**b**) comparison of CV curve of the samples, (**c**) CV curves of the filler-free PAN/PVdF/$LiClO_4$ polymer films over 50 cycles, and (**d**) CV curves of the best-performing PAN/PVdF/$LiClO_4$/LLTO (10 wt%) composite polymer electrolytes over 50 cycles

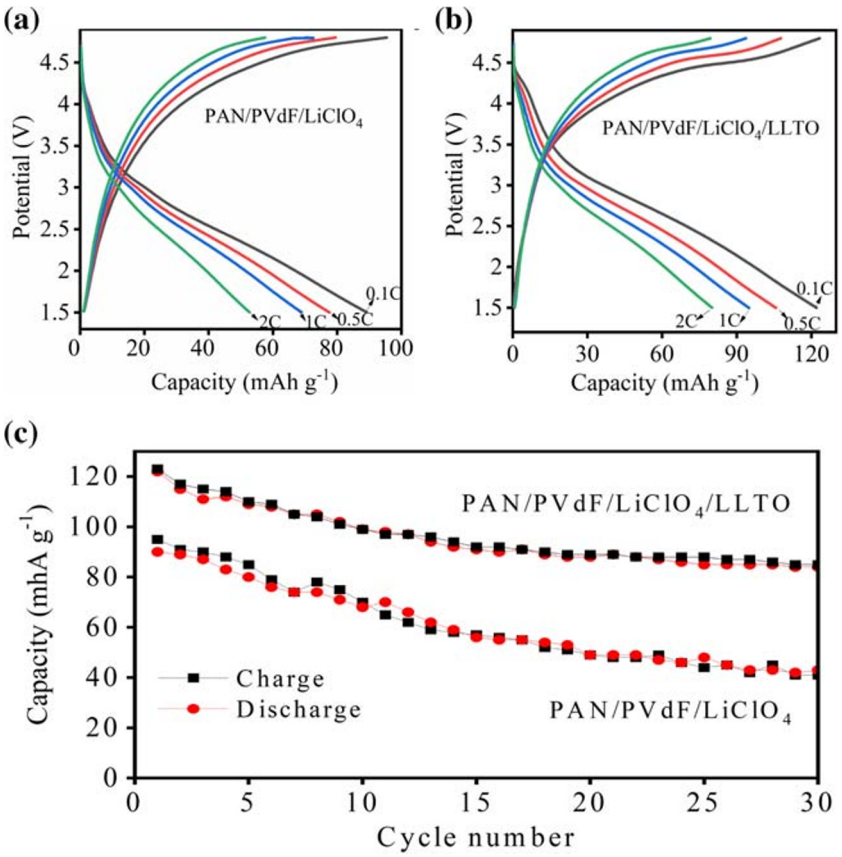

Fig. 9 (**a**, **b**) The galvanostatic charge/discharge curves of PAN/PVdF/$LiClO_4$ and best-performing PAN/PVdF/$LiClO_4$/LLTO (10 wt%) composite polymer electrolytes with different C rates (0.1, 0.5, 1, and 2C) in the potential range of 1.5–4.8 V and (**c**) the cycling stability of the solid polymer electrolytes for 30 charge/discharge cycles at 0.1C rate

$LiClO_4$/LLTO composite polymer electrolyte provides a large electrochemical stability window that can be used as a high-voltage solid electrolyte for the production of advanced all-solid-state batteries.

The cyclic voltammetry has been performed to evaluate the electrochemical performance of the filler-free and best-performing PAN/PVdF/$LiClO_4$/LLTO (10 wt%) composite electrolytes with potential between 1.5 and 5 V at a scan rate of 10 mV s^{-1}. Figure 8 b shows the comparison of first cycle of the CV profile. The PAN/PVdF/$LiClO_4$/LLTO (10 wt%) shows higher redox area and peak current than PAN/PVdF/$LiClO_4$ polymer electrolytes. Further, cycling stability of the solid polymer electrolytes has been tested over 50 cycles and depicted in Fig. 8 c and d. The area of the CV profile in filler-free PAN/PVdF/$LiClO_4$ sample decreases with increasing the cycle number which demonstrates its poor electrochemical performance. The PAN/PVdF/$LiClO_4$/LLTO (10 wt%) composite shows a similar CV profile after 50 cycles without much change in the redox peak current, peak potential, and area within the CV curves. It is revealed that the PAN/PVdF/$LiClO_4$/LLTO composite solid polymer delivered better cycling stability and electrochemical performance than filler-free PAN/PVdF/$LiClO_4$ system. In addition, the high enclosed area of the CV leads to exhibit high specific capacity [57].

The galvanostatic charge/discharge test has been performed for the PAN/PVdF/$LiClO_4$ and best-performing PAN/PVdF/$LiClO_4$/LLTO composite samples with different C rates as depicted in Fig. 9 a and b. The PAN/PVdF/$LiClO_4$/LLTO composite cathode delivered good discharge capacities of 122, 105, 94, and 80 mAh g^{-1} at current rates of 0.1, 0.5, 1, and 2C, which are better than PAN/PVdF/$LiClO_4$ solid polymer electrolyte (89, 77, 69, and 53 at 0.1, 0.5, 1, and 2C). Figure 9 c shows the cycling performance of the filler-free PAN/PVdF/$LiClO_4$/LLTO solid polymer electrolytes over 30 charge/discharge cycles at a current rate of 0.1C. It is noted that the optimum composition (10 wt%) of LLTO-incorporated PAN/PVdF/$LiClO_4$ exhibits the higher discharge capacity of 80 mAh g^{-1} after 30 charge-discharge cycles when compared with filler-free sample (43 mAh g^{-1}). The superior electrochemical cycling stability and rate performance of the PAN/PVdF/$LiClO_4$/LLTO composite solid polymer electrolyte is attributed to the excellent ionic conductivity and low activation energy. In the present research, LLTO nanoparticles are used as active fillers to boost the electrochemical performance of the hybrid PAN/PVdF/$LiClO_4$/LLTO polymer electrolyte. In addition, the LLTO has an A-site-deficient perovskite structure and hopping of mobile ions in the bottle neck size of TiO_6 octahedra in the LLTO cage producing additional lithium-ion conductive channels in the crystalline phase, which in turn increases the electrochemical stability of the composite sample. Moreover, it increases the rate of Li-ions hoping among energetically favourable sites that could result in low activation energy in the composite solid polymer electrolytes [22, 58]. The blending of LLTO nanoparticles with hybrid PAN/PVdF/$LiClO_4$ solid polymer electrolyte not only enriches the concentration of free lithium ions but also develops Li-ion conduction channels within the crystalline framework. The sufficient amount of LLTO nanoparticles incorporated into PAN/PVdF/$LiClO_4$ substantially improved ion conductivity, electrochemical cycling, and rate stability.

Conclusion

The PAN/PVdF/$LiClO_4$/LLTO composite solid polymer electrolytes have been fabricated using simple solution casting technique. The XRD study shows that the crystallinity of the PAN/PVdF host is significantly reduced by the addition of LLTO nanoparticles. The SEM micrograph shows that the addition of appropriate quantity of LLTO nanoparticles causes better morphology with less aggregation of nanoparticles. The FTIR study proved the dispersion of LLTO in the polymer matrix to form PAN/PVdF/$LiClO_4$/LLTO composites. The 10 wt% LLTO nanoparticles incorporated PAN/PVdF/$LiClO_4$ electrolyte delivered an excellent ionic conductivity of 1.43×10^{-3} S cm^{-1} which is far better than PAN/PVdF/$LiClO_4$ complex (10^{-5} S cm^{-1}). The PAN/PVdF/$LiClO_4$/LLTO composite cathode delivered good discharge capacities of 122, 105, 94, and 80 mAh g^{-1} at current rates of 0.1, 0.5, 1, and 2C, respectively. The optimum composition (10 wt%) of LLTO nanoparticles embedded in PAN/PVdF/$LiClO_4$ significantly improved ion conductivity, electrochemical stability window, and cycling performance. The hybrid PAN/PVdF/$LiClO_4$/LLTO nanocomposite is a promising candidate to use as a solid polymer electrolyte for the development of high energy density all-solid-state batteries.

Acknowledgments Mr. P. Sivaraj would like to thank the Council of Scientific Industrial Research (CSIR), Govt. of India, New Delhi, for providing the necessary financial support through the Senior Research Fellowship (SRF) (File No: 09/0472(181)-2018-EMR-I) for the present work.

Compliance with ethical standards

Conflict of interest The authors declare that they have no conflict of interest.

References

1. Tarascon JM, Armand M (2001) Issues and challenges facing rechargeable lithium batteries. Nature 414(6861):359–367
2. Belous A, Kolbasov G, Kovalenko L, Boldyrev E, Kobylianska S, Liniova B (2018) All solid-state battery based on ceramic oxide electrolytes with perovskite and NASICON structure. J Solid State Electrochem 22(8):2315–2320

3. Isikli S, Ryan KM (2020) Recent advances in solid-state polymer electrolytes and innovative ionic liquids-based polymer electrolyte systems. Curr Opin Electrochem 21:188–191
4. Hsu ST, Binh TT, Ramesh S, Hanh TTN, Arunkumar R, Ming-Yu L, Sheng-Shu H, Yuh-Lang L, Hsisheng T (2020) Free-standing polymer electrolyte for all-solid-state lithium batteries operated at room temperature. J Power Sources 449:227518
5. Florjanczyk Z, Zygado-monikowska E, Ostrowska J, Frydrych (2014) A solid polymer electrolytes based on ethylene oxide polymers. Polimery 1:80–87
6. Chandra Sekhar P, Naveen Kumar P, Sharma AK (2012) Effect of plasticizer on conductivity and cell parameters of (PMMA+ $NaClO_4$) polymer electrolyte system. J Appl Phys 2:1–6
7. Wright PV, Zheng Y, Bhatt D, Richardson T, Ugar G (1998) Supramolecular order in new polymer electrolytes. Polym Int 47(1):34–42
8. Gupta RK, Jung HY, Whang CM (2002) Transport properties of a new Li^+ ion-conducting ormolyte:$(SiO_2$–PEG)–$LiCF_3$ SO_3. J Mater Chem 12(12):3779–3782
9. Sun J, Liao X, Minor AM, Balsara NP, Zuckermann RN (2014) Morphology-conductivity relationship in crystalline and amorphous sequence-defined peptoid block copolymer electrolytes. J Am Chem Soc 136(42):14990–14997
10. Arya A, Sharma AL (2019) Electrolyte for energy storage/conversion (Li^+, Na^+, Mg^{2+}) devices based on PVC and their associated polymer: a comprehensive review. J Solid State Electrochem 23(4):997–1059
11. Egashira M, Todo H, Yoshimoto N, Morita M (2008) Lithium ion conduction in ionic liquid-based gel polymer electrolyte. J Power Sources 178(2):729–735
12. Li YH, Wu XL, Kim JH, Xin S, Su J, Yan Y, Lee JS, Guo YG (2013) A novel polymer electrolyte with improved high-temperature-tolerance up to 170 1C for high- temperature lithium-ion batteries. J Power Sources 244:234–239
13. Sharma JP, Sekhon SS (2007) Nanodispersed polymer gel electrolytes: conductivity modification with the addition of PMMA and fumed silica. Solid State Ionics 178(5-6):439–445
14. Wu N, Cao Q, Wang X, Li X, Deng H (2011) A novel high-performance gel polymer electrolyte membrane basing on electrospinning technique for lithium rechargeable batteries. J Power Sources 19:8638–8643
15. Kuo PL, Wu CA, Lu CY, Tsao CH, Hsu CH, Hou SS (2014) High performance of transferring lithium ion for polyacrylonitrile-interpenetrating crosslinked polyoxyethylene network as gel polymer electrolyte. ACS Appl Mater Interfaces 6(5):3156–3162
16. Zenghao W, Yongshuai X, Chonghe X, Shuying S, Lin W, Guanghui Z, Xinqiang W, Luyi Z (2019) Dong X zirconia fiber membranes based on PVDF as high-safety separators for lithium-ion batteries using a papermaking method. J Solid State Electrochem 23:269–276
17. Raghavan P, Manuel J, Zhao XH, Kim DS, Ahn JH, Nah C (2011) Preparation and electrochemical characterization of gel polymer electrolyte based on electrospun polyacrylonitrile nonwoven membranes for lithium batteries. J Power Sources 196(16):6742–6749
18. Appetecchi GB, Croce F, Persi L, Ronci F, Scrosati B (2000) Investigation on the stability of the lithium-polymer electrolyte interface. J Electrochem Soc 14:4448–4452
19. Wang YJ, Pan Y, Kim D (2006) Conductivity studies on ceramic $Li_{1.3}Al_{0.3}Ti_{1.7}$ $(PO_4)_3$-filled PEO-based solid composite polymer electrolytes. J Power Sources 159(1):690–701
20. Balazs AC, Emrick T, Russell TP (2006) Nanoparticle polymer composites: where two small worlds meet. Science 314(5802): 1107–1110
21. Inugama LC, Itoh M, Nakamura T, Uchida T, Ikuta H, Wakihara M (1993) High ionic conductivity in lithium lanthanum titanate. Solid State Commun 86(10):689–693
22. Abhilash KP, Christopher Selvin P, Nalini B, Somasundaram K, Sivaraj P, Chandra Bose A (2016) Study of the temperature dependent transport properties in nanocrystalline lithium lanthanum titanate for lithium ion batteries. J Phys Chem Solids 91:114–121
23. Sun L, Shi Z, Wang H, Zhang K, Dastan D, Sun K, Fan R (2020) Ultrahigh discharge efficiency and improved energy density in rationally designed bilayer polyetherimide–$BaTiO_3$/P (VDF-HFP) composites. J Mater Chem A 8(11):5750–5757
24. Sun L, Shi Z, Liang L, Wei S, Wang H, Dastan D, Sun K, Fan R (2020) Layer-structured $BaTiO_3$/P (VDF–HFP) composites with concurrently improved dielectric permittivity and breakdown strength toward capacitive energy-storage applications. J Mater Chem C 8(30):10257–10265
25. Sivaraj P, Abhilash KP, Nalini B, Christopher Selvin P, Yadav SK, Goel S (2020) Insight into cations substitution on structural and electrochemical properties of nanostructured Li_2FeSiO_4/C cathodes. J Am Ceram Soc 103(3):1685–1697
26. Dastan D (2017) Effect of preparation methods on the properties of titania nanoparticles: solvothermal versus sol–gel. Appl Phys A Mater Sci Process 123:1–13
27. Costa CM, Rodrigues LC, Sencadas V, Silva MM, Rocha JG, Lanceros MS (2012) Effect of degree of porosity on the properties of poly (vinylidene fluoride–trifluorethylene) for Li-ion battery separators. J Membr Sci 407:193–201
28. Zhong S, Sun C, Gao Y, Cui X (2015) Preparation and characterization of polymer electrolyte membranes based on silicon-containing core-shell structured nanocomposite latex particles. J Power Sources 289:34–40
29. Choi SW, Kim JR, Jo SM, Lee WS, Kim YR (2005) Electrochemical and spectroscopic properties of electrospun PAN-based fibrous polymer electrolytes. J Electrochem Soc 152: 989
30. Cai X, Lei T, Sun D, Lin L (2017) A critical analysis of the α, β and γ phases in poly (vinylidene fluoride) using FTIR. RSC Adv 7(25): 15382–15389
31. Lei T, Cai X, Wang X, Yu L, Hu X, Zheng G, Wenlong L, Lingyun W, Dezhi W, Daoheng S, Liwei L (2013) Spectroscopic evidence for a high fraction of ferroelectric phase induced in electrospun polyvinylidene fluoride fibers. RSC Adv 3(47):24952–24958
32. Anantha Iyenger G, Padmanabhan S, Kalayil Manian M, Jin Hee N, Sang Ho K, Chul-Gyun H, Kwang-Pill L (2008) Development of electrospun PVdF/PAN membrane-based polymer electrolytes for lithium batteries. J Membr Sci 325:683–690
33. Chauhan D, Afreen S, Mishra S, Sankararamakrishnan N (2017) Synthesis, characterization and application of zinc augmented aminated PAN nanofibers towards decontamination of chemical and biological contaminants. J Ind Eng Chem 55:50–64
34. Sim LH, Gan SN, Chan CH, Yahya R (2010) ATR-FTIR studies on ion interaction of lithium perchlorate in polyacrylate/poly (ethylene oxide) blends. Spectrochim Acta A Mol Biomol Spectrosc 76(3-4): 287–292
35. Yang CL, Li ZH, Li WJ, Liu HY, Xiao QZ, Lei GT, Ding YH (2015) Batwing-like polymer membrane consisting of PMMA-grafted electrospun PVdF–SiO_2 nanocomposite fibers for lithium-ion batteries. J Membr Sci 495:341–350
36. Jie J, Liu Y, Cong L, Zhang B, Lu W, Zhang X, Liu J, Xie H, Sun L (2020) High-performance PVDF-HFP based gel polymer electrolyte with a safe solvent in Li metal polymer battery. J Energy Chem 49:80–88
37. Zhang YZ, Chan CK (2003) Observations of water monomers in supersaturated $NaClO_4$, $LiClO_4$, and $Mg(ClO_4)_2$ droplets using Raman spectroscopy. J Phys Chem A 107(31):5956–5962
38. Hu W, Li T, Liu X, Dastan D, Ji K, Zhao P (2020) 1550 nm pumped upconversion chromaticity modulation in Er^{3+} doped double

perovskite $LiYMgWO_6$ for anti-counterfeiting. J Alloys Compd 818:152933
39. Dastan D, Panahi SL, Chaure NB (2016) Characterization of titania thin films grown by dip-coating technique. J Mater Sci Mater Electron 27:12291–12296
40. Kumar PM, Badrinarayanan S, Sastry M (2000) Nanocrystalline TiO_2 studied by optical, FTIR and X-ray photoelectron spectroscopy: correlation to presence of surface states. Thin Solid Films 358(1-2):122–130
41. Abhilash KP, Sivaraj P, Christopher Selvin P, Nalini B, Somasundaram K (2015) Investigation on spin coated LLTO thin film nano-electrolytes for rechargeable lithium ion batteries. Ceram Int 41(10):13823–13829
42. Pickup PG (1990) Alternating current impedance study of a polypyrrole-based anion-exchange polymer. Chem Soc Faraday Trans 86(21):3631–3636
43. Mecdonald JR (1987) Impedance spectroscopy. Wiley, New York
44. Wieczorek W, Florjanczyk Z, Stevens JR (1995) Composite polyether based solid electrolytes. Electrochim Acta 40(13-14): 2251–2258
45. Dawar A, Chandra A (2012) Electric field driven fractal growth in polymer electrolyte composites: experimental evidence of theoretical simulations. Phys Lett A 376(47-48):3604–3608
46. Chiang CY, Reddy JM, Chu PP (2004) Nano-tube TiO_2 composite $PVdF/LiPF_6$ solid membranes. Solid State Ionics 175(1-4):631–635
47. Chu PP, Reddy JM, Kao HM (2003) Novel composite polymer electrolyte comprising mesoporous structured SiO_2 and PEO/Li. Solid State Ionics 156(1-2):141–153
48. Romero M, Faccio R, Mombru AW (2016) Enhancement of lithium conductivity and evidence of lithium dissociation for LLTO-PMMA nanocomposite electrolyte. Mater Lett 172:1–5
49. Wang C, Zhang X-W, John Appleby A (2005) Solvent-free composite, PEO-ceramic fiber/mat electrolytes for lithium secondary cells. J Electrochem Soc 152(1):205–209
50. Liu W, Liu N, Sun J, Hsu P-C, Li Y, Lee H-W, Cui Y (2015) Ionic conductivity enhancement of polymer electrolytes with ceramic nanowire fillers. Nano Lett 15(4):2740–2745
51. Zhu X, Yang J, Dastan D, Garmestani H, Fan R, Shi Z (2019) Fabrication of core-shell structured Ni@ $BaTiO_3$ scaffolds for polymer composites with ultrahigh dielectric constant and low loss. Compos Part A 125:105521
52. Agrawal RC, Pandey GP (2008) Solid polymer electrolytes: materials designing and all-solid-state battery applications: an overview. J Phys D Appl Phys 41(22):223001
53. Subba Reddy CV, Sharma AK, Narasimla Rao VVR (2003) Conductivity and discharge characteristics of polyblend (PVP+ PVA+ KIO_3) electrolyte. J Power Sources 114(2):338–345
54. Shan K, Yi ZZ, Yin XT, Dastan D, Garmestani H (2020) Y-doped $CaZrO_3/Co_3O_4$ as novel dense diffusion barrier materials for limiting current oxygen sensor. Dalton Trans 49(25):8549–8556
55. Dhatarwal P, Sengwa RJ (2020) Dielectric relaxation, Li-ion transport, electrochemical, and structural behaviour of PEO/PVDF/$LiClO_4/TiO_2$/PC-based plasticized nanocomposite solid polymer electrolyte films. Compos Commun 17:182–191
56. Jamalpour S, Ghahramani M, Ghaffarian SR, Javanbakht M (2020) The effect of poly(hydroxyl ethyl methacrylate) on the performance of PVDF/P(MMA-co-HEMA) hybrid gel polymer electrolytes for lithium ion battery application. Polymer 195:122427
57. Zuo H, Fu W, Fan R, Dastan D, Wang H, Shi Z (2020) Bilayer carbon nanowires/nickel cobalt hydroxides nanostructures for high-performance supercapacitors. Mater Lett 263:127217
58. Park M, Zhang X, Chung M, Less GB, Sastry AM (2010) A review of conduction phenomena in Li-ion batteries. J Power Sources 195(24):7904–7929